A Model of Quadrotor UAV Power Consumption and Its Performance Across a Range of Flight Conditions

Alexander B. Faustino, Joshua Y Yuan, Julian Carter, Jacob Hawkins, Abhay Patel and Timothy Bretl

***Abstract*— In this paper, we present an updated parametric model of quadrotor power consumption and characterize the performance of this model in hardware experiments. Like other existing power models that have been used both for quadrotors and general rotorcraft, ours can be expressed as the sum of four terms—induced, parasitic, profile, and climb power—that depend on estimates of the aerodynamic forces and moments acting on the quadrotor. We measure the accuracy of our full model across a wide range of flight conditions and also conduct an ablation study to show the relative contribution of each term, concluding that this contribution strongly depends on the ground velocity of the quadrotor. Both our dataset and code are freely available as a benchmark to facilitate future work in this area.**

I. INTRODUCTION

Even though quadrotor helicopters have become the dominant small unmanned aerial vehicle (UAV) for both research and commercial users, the platform's problem with power efficiency persists. In addition to available LiPo battery technology, general rotor vehicle inefficiency when operating at or near hover [1] is one of the main driving issues behind this problem. Because quadrotors are often at or near hover in application, power systems often require 25-30% of the mass budget to achieve 15-18 minute flight times [2]. The problem of quadrotor power efficiency therefore creates a practical limit on the platform's utility.

Currently, most approaches to solving this problem can be classified into the development of either hardware, algorithm (software) [3], [4], [5], or bio-inspired/hybrid systems. Traditionally, the bulk of work done to increase quadrotor efficiency is in the first category. Efforts here consist mostly of reducing the weight of materials such as the airframe, sensors, and power electronics. The second category contains methods that incorporate vehicle power consumption into cost functions of existing optimal planning and control algorithms. Finally, the third category often produces novel systems that increase efficiency by transitioning to another dynamic mode such as perching, walking, or rolling. In [6], Karydis et al. provide a thorough review of promising work in all three categories.

This paper contributes to the second category, the popularity of which has grown in recent years due to the increased capabilities of onboard computers. Since the majority of algorithmic approaches are model-based, their performance is directly related to how well their power consumption model can estimate the true power consumed in actual flight. Several white box [7], [8] and black box [3], [9] models have been proposed in recent years each with their own drawbacks.

The authors are with the Department of Aerospace Engineering, Coordinated Science Laboratory, University of Illinois at Urbana-Champaign, Champaign, IL 61801, USA {afausti2, jyyuan2, julianc2, jacobrh3, abhaysp2, tbretl}@illinois.edu

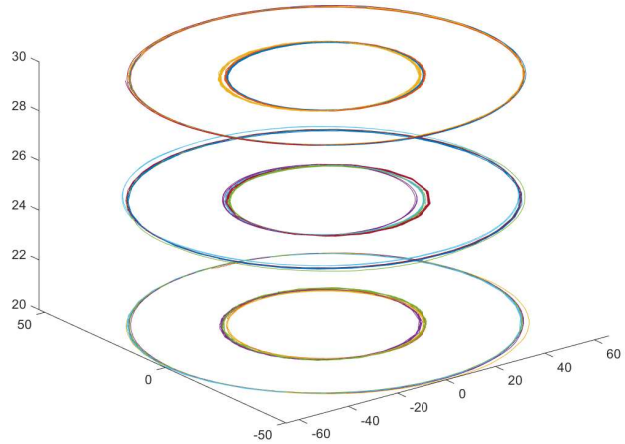

Fig. 1. Position data from all our flight experiments. With 2 orbit radii, 3 altitudes, and 5 linear ground velocities we collected data for 30 different trajectories. Each trajectory was flown for approximately 120 seconds giving us 97 complete orbits to analyze. All flight data and our ROS package can be found at https://github.com/alex-faustino/brg-qr-OptEnd.

The benefit of black box models is that they remove the need for a theoretical model, which would require determining numerous physical parameters about the quadrotor. However, they do not generalize to any desired trajectory; this constrains motion planning methods to the set of predetermined models. While these models have shown promise in implementation, this paper focuses on the study of white box models.

White box models primarily consist of summing some combination of the four major sources of aerodynamic power – induced, parasitic, profile, and climb – which are each covered in more detail in IV. Depending on which terms a model includes and how it approximates them, the model either sacrifices accuracy or requires several parameters to be identified about the quadrotor beforehand.

This work has three major contributions

1) Provide an updated white box model for quadrotor power consumption that exceeds existing model performance.
2) Characterize how the model's terms contribute to its accuracy through an ablation study of outdoor flight experiments.

Preprint submitted to IEEE Robotics and Automation Letters as Submission for RA-L and ICRA
Received September 10, 2019 17:30:26 PST

3) Provide the data from these experiments as a data set for future work on outdoor quadrotor flight problems.

The remainder of the paper is organized as follows: Section II further details existing methods that use black box or white box power consumption models; Section III contains the derivation of the quadrotor model specific to these experiments; Section IV contains the details and derivation of each term in the power consumption model; Section V describes our flight experiments; Section VI presents the outcomes and analysis of our findings; Section VII concludes with a discussion of practical applications.

II. Related Work

A. Existing white box models

White box models for quadrotor power consumption are derived from theoretical models for general rotorcraft, mainly presented by Leishman [1]. Leishman's full model has aerodynamic power required for a steady maneuver equivalent to the sum of induced power, parasitic power, profile power, and power required to climb. Aerodynamic power is then scaled by an efficiency factor to convert to electrical power consumed. The individual power terms can be approximated, simplified, or assumed negligible to reduce model complexity. Which of these terms is included and how they are simplified is the main difference between the existing white box models implemented specifically for quadrotors.

A nearly comprehensive model for power consumption is given by Liu et al. [7]. Their model contains three of the four terms from Leishman's model relevant to quadrotors: induced, profile, and parasitic, while neglecting the power required to climb. Somewhat similar to the black box models, their model requires initially collecting flight data to numerically determine seven constants. Their model is validated by flying a known trajectory and comparing the estimate of power to the actual power measured onboard. Our experiments are a natural extension to this validation, as we fly similar trajectories with more parameter variation. What differs is that we analyze how the individual terms contribute to the estimate's accuracy rather than just determining the accuracy.

In [10] Bangura and Mahony present a model for mechanical power produced by the rotors as the integral part of their nonlinear dynamic model. They draw on the previous work by [1] and [11] to derive a model that more accurately depicts the relationship between the rotors' mechanical and aerodynamic characteristics and the dynamics of the whole body during aggressive maneuvers. While this model has seen success in implementation, the traditional thrust-and-torque-based nonlinear model is still the most prevalently implemented.

B. Trajectory optimization

Ware and Roy [4] incorporate urban wind data to find more efficient trajectories between two points in the urban canopy layer. Using the wind's prevailing speed and direction above the surrounding buildings as the input to a CFD solver, they generate a grid with 1 m resolution. Similar to [3] they create a graph for a fixed altitude such that each interior node has eight edges. Using the wind vector, v_w, from the CFD solution, they can then choose an upper and lower bounded ground velocity, v_g, for the quadrotor such that it minimizes:

$$E_i = \frac{T(v_i + v_\infty \sin\alpha)(v_g - v_w)\|d\|}{v_g}$$

where $\|d\|$ is the Euclidean distance between the two nodes. They address the acceleration problem encountered by [3] by constraining the change in velocity, Δv_g, between edges. Their simulation results show that wind aware planning uses less power than wind naive planning and highlights the importance of having an estimate of the local wind field. We see in the expression for energy consumption that they are only using the dragless model or P_{ind} to minimize power along an edge. We show in Section VI that including more terms in their power model, specifically a term for parasitic power, could improve their results.

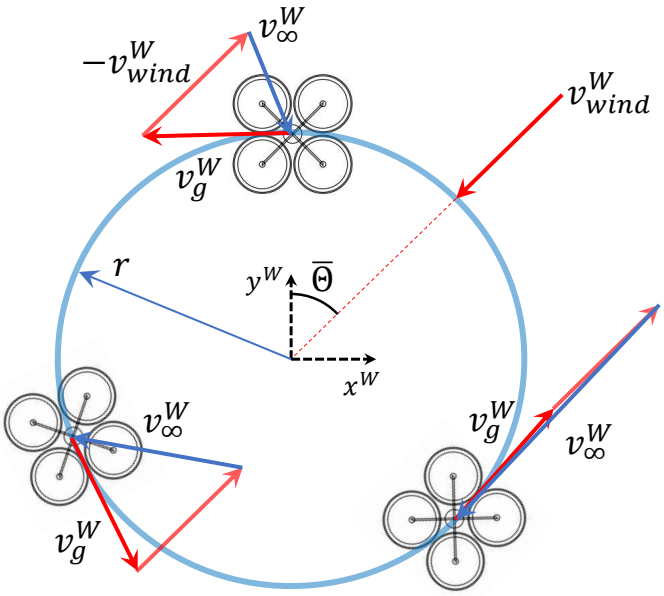

Fig. 2. Definition of the coordinates used in our analysis. Frame W is defined as a NEU world frame. Frame B (not shown) is attached to the quadrotor's center of mass. Keeping with convention, z^B points down and x^B points forward so that positive pitch angles, θ, correspond to pitching up. We define α as the angle between $\mathbf{v}_\infty^W$ and the rotor plane and $\mathbf{f}_D^W$ so that its direction is always equivalent to v_∞^W. We define the radial position in the orbit by finding the mean wind heading for each experiment, $\bar{\Theta}$, and taking that as 0 radians. We can also see that $\mathbf{v}_\infty^W$ and α vary as the quadrotor moves around the orbit.

III. Quadrotor Dynamic Model

In this section we derive our version of the standard quadrotor dynamic model given in [12] and [13] specific to the assumptions of level flight and $x^W \times y^W$ planar wind.

A. Quadrotor dynamics

We define two frames of reference, the NEU world frame, W, and the body fixed frame, B, attached to the quadrotor's

center of mass. We also define R, a rotation matrix that describes the orientation of B in W; $q^w = \left(x^W, y^W, z^W\right)$, a vector that gives the Cartesian position of B in W; and ω^B, a vector that describes the angular velocity of B with respect to W in the body frame. We parameterize R by the XYZ Euler angle sequence $\Theta = (\phi, \theta, \psi)$ corresponding to roll, pitch, and yaw respectively.

Assuming all four rotors are identical and neglecting blade flapping, each rotor will produce a thrust, $f_j^B \propto \sigma_j$, where σ_j is the spin rate of the rotor. Additionally, each rotor will produce a torque, τ_j^B, around each axis of B. Torques about x^B and y^B are moments proportional to σ_j, whereas torques about z^B are pure torques proportional to the difference in spin rate between a rotor and its counter-rotor (i.e. $\sigma_2 - \sigma_4$ and $\sigma_1 - \sigma_3$).

We can then describe the translational and rotational dynamics of the quadrotor as a set of Newton-Euler equations

$$m\ddot{\mathbf{q}}^W = R\sum \mathbf{f}_j^B + \mathbf{f}_D^W - m\mathbf{g}^W \tag{1}$$

$$I^B\dot{\omega}^B = -\omega \times I^B\omega^B + \sum {\tau_j}^B \tag{2}$$

Where I^B is the rotational inertia matrix, which is diagonal when the quadrotor is axisymmetric, the gravity vector is $\mathbf{g}^W = (0, 0, 9.8066)$ ms^{-2}, and m is the mass of the quadrotor in kilograms.

B. Assumption of level flight and planar wind

By assuming level flight and that v_{wind} is always on the $x^W \times y^W$ plane, we can make two simplifications to reduce our power model's number of parameters. First, rather than having to determine the angle of attack, α, we can approximate its cosine and sine with (3) and (4).

$$\cos\alpha = \cos\phi\cos\theta \tag{3}$$

$$\sin\alpha = \sin\phi\sin\theta \tag{4}$$

Second, using (3) we can approximate the total thrust output by all four rotors, T, with just the roll and pitch angles.

$$T = \frac{mg}{\cos\phi\cos\theta} \tag{5}$$

This means that our model requires no information about rotor spin rates to predict power consumption.

C. Drag model

Differing from [5] and [14], we approximate our drag force with a function cubic in v_∞ rather than quadratic. We did this to avoid overestimating the drag force at lower v_∞ as shown in Fig. 3. We find that a cubic drag model reduces the error in $\hat{P}$ by 28% on average across all our experiments.

$$\mathbf{f}_D^W = \left(\mu_1 v_\infty + \mu_2 v_\infty^2 + \mu_3 v_\infty^3\right)\frac{\mathbf{v}_\infty}{v_\infty} \tag{6}$$

Where μ_1, μ_2, and μ_3 are experimentally determined drag coefficients selected to make (6) approximate a more complex drag model such as the ones presented in [15], [10], or [16]. We assume that $\mathbf{f}_D^W$ is always co-linear with $\mathbf{v}_\infty^W$ and acts at the quadrotor's center of mass, producing no moments.

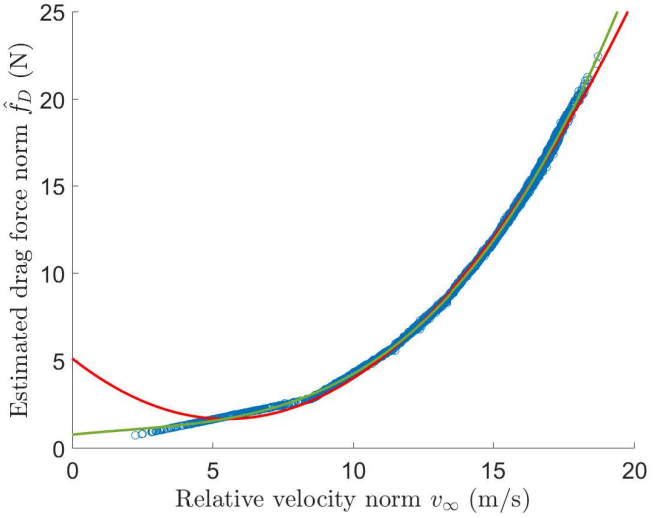

Fig. 3. Here we see that the quadratic fit (red) overestimates drag at lower v_∞, whereas the cubic fit (green) closely matches the regression data for the whole range of v_∞. The regression data was collected on level flights not in our experimental set; corresponding drag estimates are based on the residual dynamics of the quadrotor, where we assume thrust and acceleration are known. Drag coefficients for our vehicle: $\mu_1 = 0.1816$, $\mu_2 = -0.02326$, and $\mu_3 = 0.004045$.

D. Wind estimation

The question of how to estimate a wind field onboard a quadrotor has been studied in great detail over the last decade, and continues to be a pressing question in aerial robotics [17], [15], [18], [19]. As seen in Section IV, our model is dependent on the output of these models to calculate the freestream velocity's norm, v_∞. For these experiments, we use the output from DJI's built-in method for estimating wind velocity and heading. The accuracy of our model is directly dependent on the accuracy of DJI's model across varied flight regimes.

IV. Power Consumption Model

In this section, we present the derivations for each term of the power consumption model based on models for general rotorcraft given in [1] and models specific to quadrotors used in [4], [20], [5], [7].

Based on the general rotorcraft models, we assume that the total aerodynamic power required is the sum of induced power, parasitic power, profile power, and power to climb in altitude. The first three terms are the power required to overcome the drag force of the same name.

$$P_{req} = P_{ind} + P_{par} + P_{pro} + P_c \tag{7}$$

A. Induced power

Simply put, all surfaces that produce lift consequently produce drag, defined as induced drag. Several sources cover this in much greater detail in general [21], specific to rotorcraft [1], and specific to quadrotors [10]. Keeping

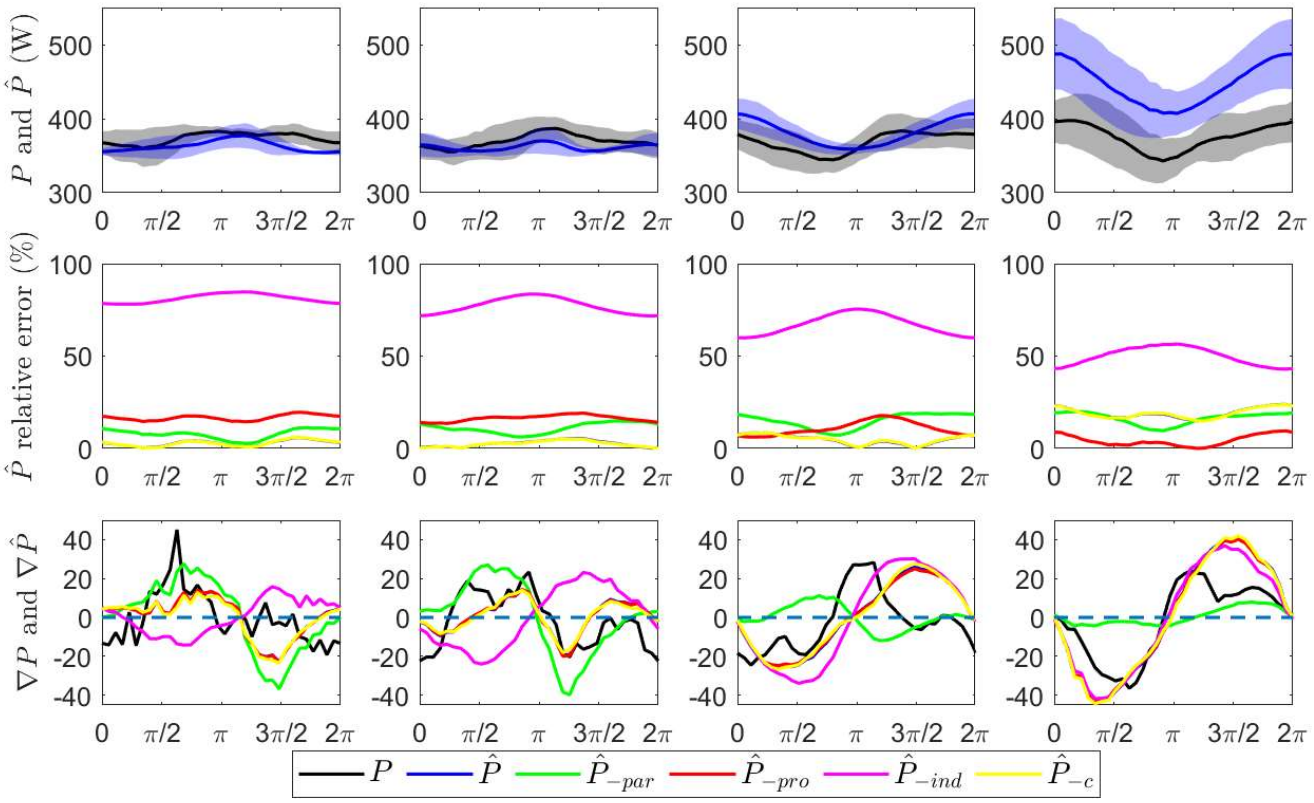

Fig. 4. Results for all non-hover flights separated by target v_g. Each plot is averaged over all altitudes and orbit radii flown. The x-axis is the quadrotor's position in the orbit in radians, descibed in Fig. 2. From left to right v_g is 2 m/s, 4 m/s, 6 m/s, and 8 m/s. The subscript of $\hat{P}$ denotes which term is removed from the model. **Top**: Mean P and $\hat{P}$ ± 1 standard deviation. As v_g increases so does the variance of $\hat{P}$. When v_g is 8 m/s we also see a large increase in error, but as seen in the plot directly below, this error can be reduced by neglecting P_{pro}. **Middle**: Relative error between model estimates and measured P. We see there is little difference between the full model and the model with P_c removed. Because all our flights were targeting a fixed altitude this is expected. It is also easy to see that the removal of P_{ind} causes the largest error magnitude over all v_g. At 8 m/s we see that the inclusion of P_{pro} degrades the accuracy of $\hat{P}$. **Bottom**: Gradient of P and $\hat{P}$ with respect to position in the orbit. At lower v_g we see that the exclusion of P_{ind} causes the gradient's sign to be incorrect the most often. As v_g increases gradient sign errors become less of an issue. There is a larger amount of error when P_{par} is removed, but in methods using gradient descent magnitude of the gradient is less important than the sign being correct.

with the existing quadrotor models, we model the induced power as (8), which is a simplified model given in [1]

$$P_{ind} = T\left(v_i + v_\infty \sin\phi \sin\theta\right) \tag{8}$$

where v_i is the velocity induced by air flowing through the rotors and is defined implicitly by [1] as

$$v_i = \frac{v_h^2}{\sqrt{\left(v_\infty \cos\alpha\right)^2 + \left(v_i + v_\infty \sin\alpha\right)^2}} \tag{9}$$

where v_h is the induced velocity at hover and can be found theoretically using (10) where r is the rotor radius. This expression for v_i can be manipulated in to a quartic function and solved numerically [11].

$$v_h = \sqrt{\frac{mg}{2\rho\pi r^2}} \tag{10}$$

B. Parasitic power

Parasitic drag comes from all nonlifting surfaces and is the predominant source of drag at higher velocities. It is often considered negligible at lower velocities for quadrotors [10]. We model the power to overcome parasitic drag as (11), which is also given in [1], and where f_D is modeled by (6).

$$P_{par} = f_D v_\infty \tag{11}$$

C. Profile power

Profile drag is generated by the transverse velocity of the rotors as they rotate. While hovering, it is equal to 0 since the opposing blades of the rotor cancel each other. We use (12) to model the power required to overcome profile drag where κ_1 and κ_2 are determined empirically [10], [7].

$$P_{pro} = \kappa_1 T^{3/2} + \kappa_2 \left(V_\infty \cos\phi \cos\theta\right)^2 T^{1/2} \tag{12}$$

Standard derivations of P_{pro} use blade element theory, which can be seen in more detail in [7]. As Liu et al. states, κ_2 is often approximately 0, so the second term of (12) can be neglected.

D. Climb power

This is the only term in our model that is not associated with overcoming drag. The power necessary to climb is

simply the weight of the quadrotor multiplied by the velocity in the global z direction as seen in (13).

$$P_c = v_z^W mg \tag{13}$$

Intuitively, it is the power required to change the quadrotor's potential energy.

E. Efficiency

To convert P_{req} to an estimate of electrical power consumed, $\hat{P}$, we join [4], [20], and [5] in assuming that all losses due to electrical components can be aggregated to one efficiency term η. This gives us (14), which is referred to as the full model for the remainder of the paper.

$$\hat{P} = \frac{1}{\eta}\left(P_{ind} + P_{par} + P_{pro} + P_c\right) \tag{14}$$

η is defined as the ratio between the theoretical power required at hover, which is found using (10), and the mean power consumed during our hover trials which are detailed in V.

V. Experiments

Our experiments consist of flying orbit trajectories, seen in Fig. 1., around a fixed point of interest. They are parameterized by the radius of the orbit, altitude, and the target linear velocity. Each of these parameters is varied independently in our experiments with linear velocities: hover, 2, 4, 6, or 8 m/s; altitudes: 20, 25, or 30 m; and orbit radius: 25 or 50 m.

The set of target linear velocities was chosen because we want to characterize how each terms' contribution in (14) vary with v_∞. By tracking a variety of v_g while orbiting, the quadrotor experiences an even larger range of v_∞. The lower and upper bound were chosen because hovering is still one of the most common modes for a quadrotor and 8 m/s is approaching the dynamic limits of most commercially available platforms.

Similarly, the set of altitudes was chosen to verify our flights were conducted high enough to avoid viscous effects from the ground. Otherwise, our planar wind field assumption would be severely inaccurate. The lower bound of this set was a safety measure to ensure the quadrotor avoided standing structures at the airfield by at least 5 m.

Lastly, we chose to fly at two different orbit radii because ϕ is smaller at larger orbits, improving our approximations of α in (14). 25 and 50 m were chosen because smaller radii make it dynamically challenging to fly at high linear velocities, whereas larger radii begin to encroach on the airfield's boundaries.

All our flights were conducted with a DJI M100 with Intel NUC7i7 onboard to handle high level control, communication with ground station, and some data logging. The majority of flight data comes from the onboard DJI flight log. The Matlab scripts and functions necessary to repeat our analysis can be found on our git repo. Parameters determined for our platform:

$$\begin{aligned} m &= 3.29 \text{ kg} \\ r &= 17.2 \text{ cm} \\ \mu_1 &= 0.182 \\ \mu_2 &= -0.023 \\ \mu_3 &= 0.004 \\ \kappa_1 &= 0.275 \end{aligned}$$

Where κ_1 was found following [7], and our determination of μ_1, μ_2, and μ_3 is described in III .

TABLE I
$\hat{P}$ MEAN NRMSE (%) FOR THE REMOVAL OF EACH TERM FROM THE MODEL

Dropped out term	Hover	2 m/s	4 m/s	6 m/s	8 m/s
none	8.36	7.22	7.06	9.15	18.30
P_{par}	13.57	11.20	12.65	15.99	18.26
P_{pro}	20.97	17.89	17.51	13.28	11.36
P_{ind}	80.70	81.86	78.12	68.44	54.73
P_c	8.46	7.31	7.12	9.19	18.37

VI. Results and Discussion

The results of our experiments are evaluated by assuming two primary use cases for a power consumption model in autonomous UAV planning and control. The first case is predicting the total power consumed by a trajectory, which requires the power consumption model to be accurate across all states in the trajectory. The second case is determining the parameters of minimal power trajectories, where the model's gradient should have the same sign as the actual power consumed gradient with respect to controllable states. For both cases, our results indicate that a hybrid model based on v_∞ may be necessary.

A. Estimating total power

As seen in Fig. 4 and Table 1, P_{ind} is by far the largest contributor to accurate estimates of power consumption, especially at lower v_g. As expected, the contribution of P_{par} increases with v_g, but is still dominated by P_{ind}. Interestingly, it is evident that the inclusion of P_{pro} degrades the estimate at greater v_g. This could be attributed to the assumption used to neglect a term discussed in IV or the method for determining the constant κ_1. Since all our flights were conducted at near-level flight, it is expected that P_c is nearly negligible.

Table 1 also shows that our full model achieves relative errors lower than previously published models. Since we did not evaluate any of these models using our data, it is not a fair comparison, but it is still worth noting until further verification. This is of particular interest to path and motion planning problems that keep a large margin of battery capacity. By having a better estimate of P, uncertainty around max flight time decreases, allowing for a larger feasible trajectory set.

B. Determining minimal power trajectories

For any application that uses gradient descent to minimize power consumption, a model that preserves the sign of the gradient with respect to the decision variables is necessary. We approximate the gradient of our model with respect to v_∞, θ, and ϕ by taking a finite difference between samples taken while orbiting. In Fig. 4, we see that removing P_{ind} causes a large amount of gradient sign error, an extremely undesirable result for methods dependent on gradient descent. Fig. 4 also shows that this problem diminishes as v_g increases, but as previously stated this magnitude of v_g approaches the current dynamic limit of commercial platforms. Based on that, P_{ind} should always be present in a model where some form of gradient descent is used.

We want to highlight the reliance of our model on accurate estimations of the 3D, time-varying wind field. We think there is room for significant improvement in solutions to this problem, particularly in the atmospheric boundary layer and urban canopies. Looking forward, it will be important to not only estimate the wind vector directly acting on the UAV, like current methods, but to predict the wind field of the entire operating area as well.

VII. Conclusion and Future Work

In this paper we presented an updated white box model for quadrotor UAV power consumption, which achieves relative errors below 12 % across a range of flight conditions. We evaluated the contribution of each term in the model with respect to accuracy of the power estimate and its gradient. By assuming level flight and planar wind, our model only depends on roll, pitch, and v_∞. We varied these parameters by flying planar orbits at different ground velocities, v_g. We showed empirically that the P_{ind} term is the greatest contributor to reducing total error across all flight regimes we studied. Agreeing with previous work we also showed that P_{par} contributes more to error reduction as v_g increases. To reduce error at larger velocities, P_{pro} should be ignored; this suggests the use of a hybrid model. Additionally, with respect to the power gradient having the correct sign, P_{ind} is extremely important at lower v_g, but is nearly negligible at larger velocities.

Moving forward, a hybrid or weighted model should be designed and validated using the data from these experiments. This new model could then be utilized as the power consumption model for power minimization methods in experiment and practice. Based on the findings of experiments in this paper, incorporating that model should reduce power consumption relative to previous implementations. Additionally, we want to focus on improving the wind estimation techniques that our model relies heavily on. Particularly, moving towards onboard estimation of low altitude and urban canopy wind fields at large. Improving methods for wind estimation will be beneficial to UAV planning problems in general not just quadrotors.

Acknowledgments

The authors would like to thank the Champaign County Radio Control Club for allowing us full use of their facilities and equipment. We would also like to thank Grayson Schaer for being the best wind boy anyone could ask for.

References

[1] G. J. Leishman, *Principles of helicopter aerodynamics*. Cambridge university press, 2000.
[2] V. Kumar and N. Michael, "Opportunities and challenges with autonomous micro aerial vehicles," *IJRR*, vol. 31, no. 11, pp. 1279–1291, 2012.
[3] C. Di Franco and G. C. Buttazzo, "Energy-aware coverage path planning of uavs." in *ICARSC*, 2015, pp. 111–117.
[4] J. Ware and N. Roy, "An analysis of wind field estimation and exploitation for quadrotor flight in the urban canopy layer," in *ICRA*. IEEE, 2016, pp. 1507–1514.
[5] A. Tagliabue, X. Wu, and M. W. Mueller, "Model-free online motion adaption for optimal range and endurance of multicopters," in *ICRA*. IEEE, 2019.
[6] K. Karydis and V. Kumar, "Energetics in robotic flight at small scales," *Interface focus*, vol. 7, no. 1, p. 20160088, 2017.
[7] Z. Liu, R. Sengupta, and A. Kurzhanskiy, "A power consumption model for multi-rotor small unmanned aircraft systems," in *ICUAS*. IEEE, 2017, pp. 310–315.
[8] N. Bezzo, K. Mohta, C. Nowzari, I. Lee, V. Kumar, and G. Pappas, "Online planning for energy-efficient and disturbance-aware uav operations," in *IROS*. IEEE, 2016, pp. 5027–5033.
[9] A. S. Prasetia, R.-J. Wai, Y.-L. Wen, and Y.-K. Wang, "Mission-based energy consumption prediction of multirotor uav," *IEEE Access*, vol. 7, pp. 33 055–33 063, 2019.
[10] M. Bangura, R. Mahony *et al.*, "Nonlinear dynamic modeling for high performance control of a quadrotor," in *ACRA*, 2012, pp. 1–10.
[11] G. Hoffmann, H. Huang, S. Waslander, and C. Tomlin, "Quadrotor helicopter flight dynamics and control: Theory and experiment," in *AIAA Guidance, Navigation and Control Conference and Exhibit*, 2007, p. 6461.
[12] G. Hoffmann, D. G. Rajnarayan, S. L. Waslander, D. Dostal, J. S. Jang, and C. J. Tomlin, "The stanford testbed of autonomous rotorcraft for multi agent control (starmac)," in *DASC*, vol. 2. IEEE, 2004, pp. 12–E.
[13] P. Pounds, R. Mahony, P. Hynes, and J. M. Roberts, "Design of a four-rotor aerial robot," in *ACRA*. Australian Robotics & Automation Association, 2002, pp. 145–150.
[14] M. Schulz, F. Augugliaro, R. Ritz, and R. D'Andrea, "High-speed, steady flight with a quadrocopter in a confined environment using a tether," in *IROS*. IEEE, 2015, pp. 1279–1284.
[15] H. Huang, G. M. Hoffmann, S. L. Waslander, and C. J. Tomlin, "Aerodynamics and control of autonomous quadrotor helicopters in aggressive maneuvering," in *ICRA*. IEEE, 2009, pp. 3277–3282.
[16] R. C. Leishman, J. C. Macdonald, R. W. Beard, and T. W. McLain, "Quadrotors and accelerometers: State estimation with an improved dynamic model," *IEEE Control Systems Magazine*, vol. 34, no. 1, pp. 28–41, 2014.
[17] S. Waslander and C. Wang, "Wind disturbance estimation and rejection for quadrotor position control," in *AIAA Infotech@ Aerospace Conference and AIAA Unmanned... Unlimited Conference*, 2009, p. 1983.
[18] J. González-Rocha, C. A. Woolsey, C. Sultan, and S. F. De Wekker, "Sensing wind from quadrotor motion," *Journal of Guidance, Control, and Dynamics*, vol. 42, no. 4, pp. 836–852, 2019.
[19] X. Xiang, Z. Wang, Z. Mo, G. Chen, K. Pham, and E. Blasch, "Wind field estimation through autonomous quadcopter avionics," in *DASC*. IEEE, 2016, pp. 1–6.
[20] N. Kreciglowa, K. Karydis, and V. Kumar, "Energy efficiency of trajectory generation methods for stop-and-go aerial robot navigation," in *ICUAS*. IEEE, 2017, pp. 656–662.
[21] J. Anderson, *Introduction to Flight*, ser. McGraw-Hill series in aeronautical and aerospace engineering. McGraw-Hill Higher Education, 2005. [Online]. Available: https://books.google.com/books?id=Hd_AR0CAmsoC